Chemical Science

ROYAL SOCIETY OF CHEMISTRY

EDGE ARTICLE

View Article Online
View Journal | View Issue

Cite this: *Chem. Sci.*, 2026, **17**, 2281

All publication charges for this article have been paid for by the Royal Society of Chemistry

Received 28th October 2025
Accepted 27th November 2025

DOI: 10.1039/d5sc08335d

rsc.li/chemical-science

Odoribacter splanchnicus lipooligosaccharide: an uncommon structure with weak immunostimulatory activity

Marta Tiemblo-Martin,†[a] Marcello Mercogliano,†[a] Kaisa Hiippala,†[b] Luca De Simone Carone,[acd] María Asunción Campanero-Rhodes,[fg] Maria Masiello,[a] Alessandro Cangiano,[ae] Antonio Molinaro,[ad] Luigi Paduano,[ae] Dolores Solís,[fg] Reetta Satokari,[b] Flaviana Di Lorenzo *[ad] and Alba Silipo *[ad]

Odoribacter splanchnicus, a prominent member of the human gut microbiota, has emerged as a promising next-generation probiotic due to its anti-inflammatory properties and association with intestinal health. While previous studies have demonstrated its ability to attenuate inflammation and protect epithelial integrity, the molecular basis underlying these effects remained elusive. In this study, we provide the first comprehensive structural and functional characterization of the *O. splanchnicus* lipooligosaccharide (LOS), a major immunomodulatory surface component. NMR spectroscopy and mass spectrometry revealed a heterogeneous LOS structure composed of a mono-phosphorylated tetra- and penta-acylated lipid A backbone and a highly branched, short core oligosaccharide featuring unique residues such as 4-lactylmannose and galactosaminuronic acid. Small-angle X-ray scattering demonstrated that the LOS self-assembles into core–shell spherical micelles, with a large oligosaccharide corona shielding the lipid A, thereby limiting its accessibility to the innate immunity TLR4/MD-2 receptor complex. Accordingly, the *O. splanchnicus* LOS exhibited minimal TLR4 activation and failed to induce IL-8 secretion in enterocyte cell lines, in stark contrast to proinflammatory *Escherichia coli* LPS; in addition, it potently antagonized *E. coli* LPS-induced inflammation. These findings identify the LOS as a key effector of the *O. splanchnicus* anti-inflammatory phenotype and support its further development as a live biotherapeutic agent.

Introduction

The gut microbiota has emerged as a vital component of host health, with changes in its composition and activity closely linked to the onset of various diseases.[1] Among the diverse microbial species inhabiting the human gut, *Odoribacter splanchnicus* has recently emerged as a promising next-generation probiotic (NGP), owing to its ability to produce short-chain fatty acids, modulate immune responses, and maintain intestinal homeostasis.[2,3] Originally isolated from human abdominal abscesses, *O. splanchnicus* is now recognized as a prevalent and metabolically active member of the gut microbial community, associated with health-promoting effects such as anti-inflammatory activity and reinforcement of the epithelial barrier.[4–6] Conversely, a reduction in its presence has been observed in several disease conditions, including inflammatory bowel disease, non-alcoholic fatty liver disease and cystic fibrosis.[7] *O. splanchnicus* was also identified as part of a core group of transferable donor-derived strains in fecal microbiota transplantation-treated ulcerative colitis patients, and colonization of mice with this bacterium led to the induction of mucosal regulatory T cells.[8,9] *In vitro* studies further demonstrated that cell-free supernatants from *O. splanchnicus* isolates exert anti-proliferative effects on human colon cancer cells.[10] More intriguingly, the outer membrane vesicles (OMVs) it produces do not elicit IL-8 secretion in intestinal epithelial cells, suggesting a remarkably low proinflammatory potential, while at the same time exhibiting protective, anti-inflammatory activity *in vitro*.[5] We also successfully formulated *O. splanchnicus*

[a]*Department of Chemical Sciences and Task Force for Microbiome Studies, University of Naples Federico II, Via Cinthia 4, Naples, 80126, Italy. E-mail: flaviana.dilorenzo@unina.it; silipo@unina.it*

[b]*Human Microbiome Research Program, Faculty of Medicine, University of Helsinki, Haartmaninkatu 8 (P O Box 63), 00014, Finland*

[c]*Department of Biology, University of Naples Federico II, Via Cinthia 4, Naples, 80126, Italy*

[d]*CEINGE Biotecnologie Avanzate Franco Salvatore, Via Gaetano Salvatore, 486, Naples, 80131, Italy*

[e]*CSGI, Center for Colloid and Surface Science, 50019 Sesto Fiorentino, Italy*

[f]*Instituto de Química Física Blas Cabrera, CSIC, Serrano 119, 28006 Madrid, Spain*

[g]*CIBER de Enfermedades Respiratorias (CIBERES), Avda Monforte de Lemos 3-5, 28029 Madrid, Spain*

† Equal contribution.

strain 57 for oral colon delivery, indicating the isolate's suitability to be developed into a live biotherapeutic agent.[11]

All these findings are especially noteworthy, considering that *O. splanchnicus* is a Gram-negative bacterium whose outer membrane is characterized by the presence of lipopolysaccharides (LPSs), microbe associated molecular patterns acknowledged as potent inducers of inflammatory responses. LPSs are tripartite molecules composed of a glycolipid moiety (lipid A), an oligosaccharide region (core OS), and a polysaccharide chain (*O*-antigen). LPS molecules comprising all three regions are referred to as a smooth-type LPS (S-LPS), whereas those lacking the *O*-antigen are known as a rough-type LPS or lipooligosaccharide (R-LPS or LOS).[12] The lipid A portion typically acts as a potent pro-inflammatory stimulus by binding to the innate immune system receptorial complex made up of Toll-Like Receptor 4/Myeloid Differentiation Protein-2 (TLR4/MD-2).[13] However, the immunological properties of an LPS are tightly linked to its chemical structure. The LPS from *Escherichia coli*, for instance, possesses structural features that make it a robust TLR4 agonist and a powerful inducer of inflammation, namely a hexa-acylated lipid A with 4 + 2 symmetry and two phosphate groups on the glucosamine disaccharide backbone.[14] In contrast, structural deviations in the lipid A moiety (as well as in the carbohydrate portion) can significantly reduce or even abrogate its pro-inflammatory activity. Therefore, an LPS can behave as a strong, weak, or even inert immunostimulant, depending on its molecular architecture.[15]

Therefore, understanding whether the LPS contributes to *O. splanchnicus* anti-inflammatory potential is critical for delineating the role of this gut bacterium as a modulator of host immune homeostasis. In this framework, we present the first structural characterization of the LOS isolated from *O. splanchnicus*, together with the evaluation of its functional effects on TLR4 signaling and intestinal epithelial cells. The immunomodulatory phenotype observed here confirmed the hypothesis that its *O. splanchnicus* LOS possesses structural features that deviate from the canonical pro-inflammatory archetype exemplified by *E. coli* and is linked to weak TLR4 activation.

Results

O. splanchnicus LOS isolation and chemical analysis

The LOS from *O. splanchnicus* was isolated following hot phenol-water extraction and further purified by enzymatic treatments and gel-filtration chromatography. Monosaccharide analysis indicated the presence of D-mannose (D-Man), D-glucosamine (D-GlcN), D-galactosaminuronic acid (D-GalNA), L-glycero-D-manno-heptose (Hep), and 3-deoxy-D-manno-oct-2-ulosonic acid (Kdo). Moreover, GC-MS analysis of the acetylated methyl glycosides revealed the presence of a hexose substituted with a lactyl moiety, which was subsequently identified by NMR as 4-O-[1-carboxyethyl]-D-mannose. The electron impact mass spectrum of this monosaccharide, analyzed as an acetylated methyl glycoside, displayed diagnostic fragment ions at *m*/*z* 375, 347, 289, 272, 213 and 142. Methylation analysis indicated the presence of 2,7-substituted heptose (2,7-Hep), terminal GalNA (*t*-GalNA), terminal Man4Lac (*t*-Man4Lac), terminal and 4-substituted Man (*t*-Man and 4-Man), 6-substituted GlcN (6-GlcN) and 5-substituted Kdo (5-Kdo). Fatty acid compositional analysis revealed the presence of anteiso-pentadecanoic acid (aC15:0), iso-C15:0 (iC15:0) and C15:0, hydroxyhexadecanoic acid [C16:0 (3-OH)], and anteiso-hydroxyheptadecanoic acid [aC17:0 (3-OH)], iC-17:0 (3-OH), and C17:0 (3-OH).

Structural determination of *O. splanchnicus* LOS

To elucidate the structure of the saccharide portion of the *O. splanchnicus* LOS, an aliquot was fully de-acylated and further purified by gel-filtration chromatography to get the pure saccharide fraction (OS_{deAc}), which was extensively studied by NMR spectroscopy, ESI-MS and tandem MS (Fig. 1 and 2). The anomeric configuration of the monosaccharide units was assigned based on $^{3}J_{H1,H2}$ and $^{1}J_{C1,H1}$ coupling constants, and further confirmed by intra-residue NOE contacts. The relative configuration of sugar residues was elucidated by analyzing vicinal $^{3}J_{H1,H2}$ coupling constants and intra-residue NOE contacts. Five spin systems were identified (Fig. 1, S1 and Table S1); all the monosaccharide residues were present as pyranose rings, as indicated by both ^{13}C chemical shift values and the long-range correlations in the HMBC spectrum between positions 1 and 5 (for Kdo between C-2 and H-6).[16]

Spin systems **H** and **N** were both gluco configured sugar residues, based on the large $^{3}J_{H,H}$ ring coupling constants and were identified as GlcpN residues based on the correlation of their H-2 resonance to nitrogen bearing carbon signals (Fig. 1 and Table S1). The intra-residue NOE contact of H-1 with H-3 and H-5, and $^{3}J_{H1,H2}$ and $^{1}J_{CH}$ values were indicative of the β-anomeric configuration of H. Conversely **N** was identified as an α-GlcN, whose anomeric configuration was determined according to $^{3}J_{H1,H2}$ and the sole H1-H2 intra-residual NOE contact. Spin system **B** was assigned to a galacto configured sugar unit as evident from the low $^{3}J_{H3,H4}$ and $^{3}J_{H4,H5}$ values (3 Hz and <1 Hz, respectively). Both $^{3}J_{H1,H2}$ and $^{1}J_{CH}$ coupling constants, together with intra-residual NOE contact of H-1 with H-2, were diagnostic for the α-configuration. In addition, and in accordance with the compositional analysis, scalar correlations between H-5 and a carboxylate group, evident from the HMBC spectra, and the correlation of the H-2 resonance with nitrogen-bearing carbon signals allowed this to be identified as a GalNA unit. Spin system **E** matched with an α-Man, with its C4 bonded to C2 of lactic acid (ether bond). The manno configuration was established by low $^{3}J_{H1,H2}$ and $^{3}J_{H2,H3}$, both below 2 Hz and diagnostic of the H-2 equatorial orientation. Spin system **A** matched with an α-heptose, whose manno configuration was established as above. Spin system **K** was assigned to the Kdo residue based on the diastereotopic methylene proton signals resonating in the high-field region of the NMR spectrum; its α-anomeric configuration was assigned on the basis of the H-3 chemical shift values (Table S1).[17] The down-field shifted carbon signals were indicative of glycosylation at position O-6 and O-1 of **N**, O-6 of **H**, O-5 and O-4 of **K**, and O-2 and O-7 of **A**, while **B** was identified as a terminal residue, in accordance

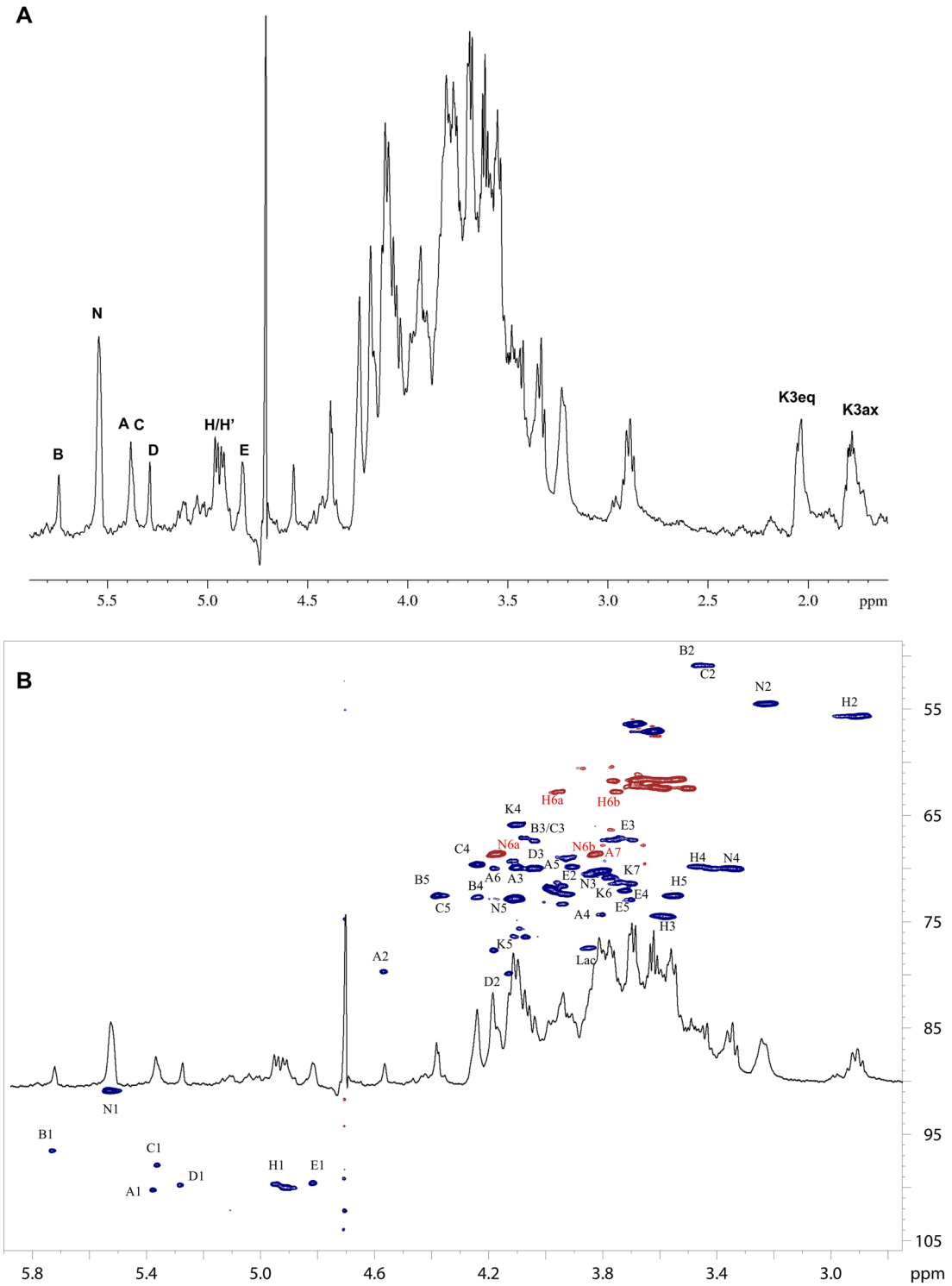

Fig. 1 (A) The ^{1}H NMR spectrum of the fully deacylated LOS (OS_{deAc}) presents anomeric signals as indicated in the inset, corresponding to those listed in Table S1. Most of the NMR signals from the sugar residues appear split because of the non-stoichiometric phosphorylation of Kdo. Additionally, the structure of OS_{deAc}, as determined through NMR analysis, is illustrated in the accompanying figure. (B) NMR structural assessment of the aliquot fully de-acylated and purified from the *O. splanchnicus* LOS (OS_{deAc}). Multiplicity edited HSQC (blue and red) NMR spectrum, assigned as attributed in Table S1.

with the methylation analysis. The analysis of the inter-residual NOE contacts (Fig. S2) helped to define the complete monosaccharide sequence of the LOS from *O. splanchnicus*. Residues β-(1 → 6) linked **H** and **N** composed the lipid A saccharide backbone. Unit **H** was substituted at position O-6 by the Kdo residue (**K**), as also confirmed by the weak downfield shift of the

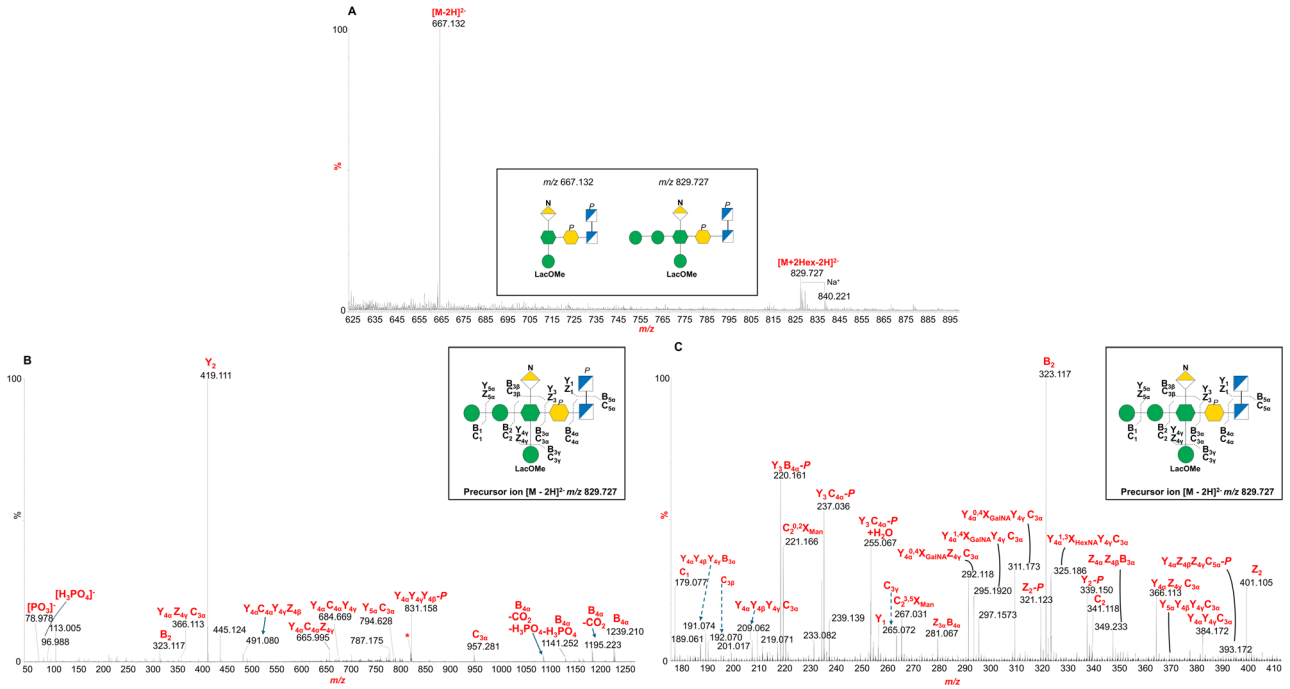

Fig. 2 (A) Enlargement of the negative-ion ESI MS spectrum of OS_{deAc}. (B and C) MS/MS spectrum, zoomed-in view, of the precursor triply charged ion at *m/z* 829.727. The proposed structure for the core oligosaccharide was drawn using the Symbol Nomenclature for Glycans (SNFG). The nomenclature of glycan fragment ions generated from the cleavage of a glycosidic bond is also reported. Symbols legend: green circle: mannose; blue/white square: glucosamine; green hexagon: heptose; yellow/white diamond: galactosaminuronic acid; yellow hexagon: Kdo; P and LacOMe stand for phosphate and the methylated lactyl moiety.

signal of C-6 **H** (Table S1), expected for the α-(2 → 6) ketosidic linkage of Kdo with the β-GlcN of the lipid A. The Kdo unit was, in turn, substituted at O-5 by the heptose residue **A**, as suggested by the corresponding inter-residue NOE contacts, together with the HMBC correlations **A1**-**K5**.

Last, residue **A** was substituted at position O-2 by the terminal GalNA residue **B**, and in position O-7 by the terminal Man4Lac residue **E**. Overall we defined the structure as shown in Scheme 1.

This structural deduction was confirmed and expanded by direct infusion ESI-MS and MS/MS analysis of OS_{deAc}. As shown in Fig. 2A, the negative-ion ESI-MS spectrum revealed a dominant double charged $[M–2H]^{2-}$ ion at *m/z* 667.132 consistent with the deacylated LOS structure. The assigned composition includes one Kdo, one heptose (Hep), one hexosaminuronic acid (HexNA), one hexose (Hex) carrying lactic acid (HexLac), one phosphate group, and one methyl group, along with a mono-phosphorylated diglucosamine backbone derived from lipid A (see below). Strikingly, a $[M–2H]^{2-}$ ion at *m/z* 829.727, consistent with the above-mentioned composition plus two other Hex units (likely mannoses, according to chemical analyses) was also detected. A related sodium adduct was also identified at *m/z* 840.1221.

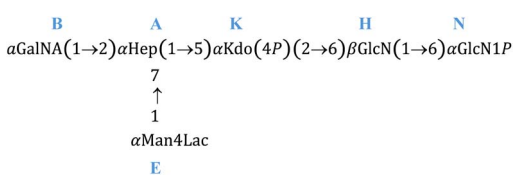

Scheme 1 Structure of the OS_{deAc} from *O. splanchnicus* obtained from the combination of chemical, NMR and MS investigations.

Negative-ion MS/MS analysis of the precursor ion at *m/z* 829.727 (Fig. 2B and C) provided key insights into the glycan sequence, confirming the structural assignment deduced by NMR and revealing the position of the two additional Hex residues, which could not be resolved by NMR alone. The MS/MS spectrum in fact revealed glycosidic and cross-ring fragments distinctive of the core region in the *m/z* 50–1250 range. The most intense peak at *m/z* 419.111 (Fig. 2B) matched with the mono-phosphorylated lipid A diglucosamine backbone (Y_2 ion) while the related $B_{4\alpha}$ fragmentation was detected at *m/z* 1239.210. Peaks attributed to ions originating from phosphate and/or carbon dioxide losses were also identified (Fig. 2B). Of note, the identification of the peak at *m/z* 265.072 (Fig. 2C) revealed that the methyl group was on the HexLac unit. The sequentiality of the two Hex was demonstrated by the intense B_2 fragment at *m/z* 323.117 (Fig. 2B and C) while their linkage to the Hep by the $C_{3\alpha}$ fragment at *m/z* 957.281, was in parallel supported by the absence of any peaks attributable to the loss of one (or two) Hex plus HexNA or HexLac. Additional fragments confirmed the peculiar highly branched oligosaccharide structure, such as the peaks at *m/z* 684.669 and *m/z* 794.628 that supported the presence of the methylated HexLac and the HexNA on the Hep moiety, in agreement with the NMR analysis. In parallel, the lipid A structure was determined by merging

data from compositional and MALDI-TOF MS analyses. In the negative-ion MALDI-TOF MS spectrum (Fig. S3) the existence of different lipid A species was shown, with two main clusters of signals differing in the number of fatty acid chains. Each group of ions exhibited mass differences indicating variation in the fatty acid chain length within the lipid A species. In detail, the most intense cluster of ions in the mass range *m*/*z* 1600–1702 was consistent with mono-phosphorylated penta-acylated lipid A species whose fatty acid distribution and composition for the ion peak at *m*/*z* 1660.1 was determined as two C17:0 (3-OH) as N-linked acyl chains, two C15:0(3-OH) as primary O-linked fatty acids and C15:0 as a secondary *O*-acyl substitution, in accordance with fatty acid compositional analysis and previously reported data on Bacteroidetes lipid A.[28–31] The cluster of ions visible in the mass range *m*/*z* 1391–1434 was attributed to mono-phosphorylated tetra-acylated lipid A species with the main ion peak at *m*/*z* 1419.0 assigned to a lipid A species possessing the above-mentioned fatty acid distribution and composition but lacking one primary O-linked C15:0(3-OH). Finally, to gain a more comprehensive structural overview, an aliquot of LOS was hydrolyzed with diluted ammonium hydroxide. This treatment selectively removed O-linked acyl chains, enabling a clearer assessment of structural variability in both the oligosaccharide and lipid A portions across the detected species. The resulting spectrum revealed that the main peaks differed predominantly in the length of the saccharide chain and the number and type of acyl chains on the lipid A moiety (Fig. 3). For instance, the most intense triply charged ion, $[M–3H]^{3-}$ at *m*/*z* 806.616, was assigned to a species composed of the complete core OS linked to a lipid A carrying two N-linked 17:0(3-OH) chains and one secondary 15:0 fatty acid. In comparison, the $[M–3H]^{3-}$ ion at *m*/*z* 891.672 was attributed to the same structure bearing an additional 16:0(3-OH) unit. Additional species were also detected, featuring lipid A with three or four acyl chains of varying lengths, associated either with the intact core OS or with truncated versions lacking the Hex residues and/or one phosphate group.

Overall, we concluded that the *O. splanchnicus* LOS is made up of a core region that was predominantly composed of a tetrasaccharide backbone bearing a phosphorylated Kdo unit, which was further substituted at position O-5 by a Hep residue. This heptose was identified as a branched monosaccharide, carrying an α-GalNA unit at position O-2 and an α-Man4Lac at position O-7. The stereochemistry of lactic acid remains to be defined. In addition, MS analysis revealed structural heterogeneity within the LOS species, with the detection of extended species bearing a disaccharide of (1 → 4)-linked hexose residues at the non-reducing end of the core OS. These additional Hex units, likely D-mannoses according to compositional analyses, are attached to position O-4 of the Hep residue, further contributing to the observed microheterogeneity. Consistent with this, integration of MS and linkage analysis data suggested that these extended species represent a minor subpopulation of the LOS, accounting for approximately 10% of the mixture. The presence of the GalNA residue in the LOS is particularly notable, as this monosaccharide is rarely observed in LOS core

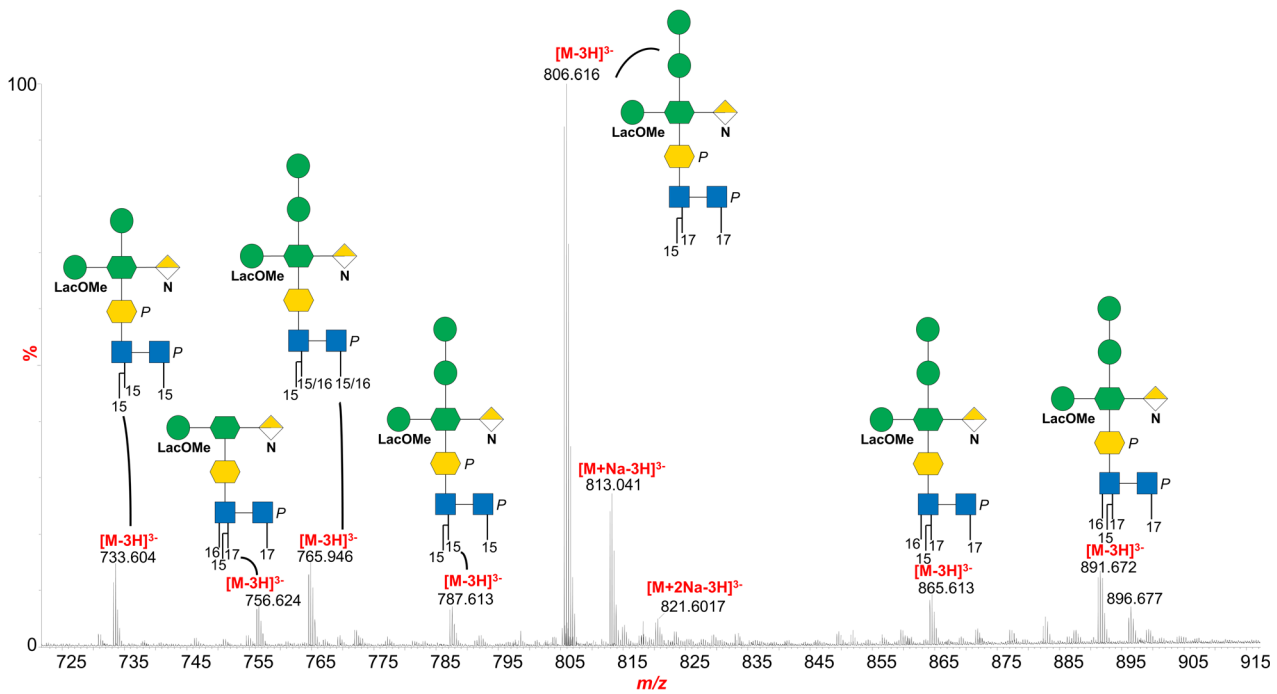

Fig. 3 Enlargement of the negative-ion ESI MS spectrum of the LOS after hydrolysis with diluted ammonium hydroxide. The proposed structure for LOS species was drawn using the Symbol Nomenclature for Glycans (SNFG). The nomenclature of glycan fragment ions generated from the cleavage of a glycosidic bond is also reported. Symbols legend: green circle: mannose; blue/white square: glucosamine; green hexagon: heptose; yellow/white diamond: galactosaminuronic acid; yellow hexagon: Kdo; P and LacOMe stand for phosphate and the methylated lactyl moiety.

oligosaccharides, though it has been reported in the *O*-antigen of *Pseudomonas aeruginosa*[18] and in the core region of *Bordetella bronchiseptica*, a respiratory pathogen in mammals including humans.[19] Remarkably, in *B. bronchiseptica*, the absence of GalNA correlates with a reduced induction of TNF-α, a key proinflammatory cytokine involved in early host defense.[19] This suggests a potential immunomodulatory role for GalNA, either direct or indirect, shaping host responses to bacterial components. Another notable peculiarity of the *O. splanchnicus* LOS is the presence of the rare sugar residue 4-Lactylmannose (4-O-[1-carboxyethyl]mannose; D-ManpLac). This residue is an uncommon substituent in bacterial polysaccharides, although it has been previously identified in the extracellular polysaccharides *Cyanospira capsulate, Mycobacterium lacticolum* 121 and the halophilic bacterium *Salinivibrio* sp. EG9S8QL.[20–22] Lactic acid itself has been described as an ether-linked substituent in various bacterial polysaccharides, most notably as an N-linked substituent in *N*-acetylmuramic acid. However, to the best of our knowledge, this is the first report of D-Man4Lac in a member of the *Bacteroidota* phylum. Given that the structural specificity of microbial glycans is intimately linked to their biological function, it is tempting to hypothesize that the presence of D-Man4Lac may be involved in bacterial recognition by host immune systems. Interestingly, *Cyanobacterium Nostoc commune* contains a different derivative, a lactylated uronic acid called "nosturonic acid",[23] and its exopolysaccharides have been extensively studied for their prebiotic functions in selectively promoting beneficial bacterial growth such as bifidobacteria and lactobacilli while inhibiting pathogenic microorganisms. This selective modulation of gut microbiota helps to maintain intestinal barrier integrity and supports host health.[24,25] In addition, several studies indicate that mannose derivatives can influence cytokine production and immune cell activation,[26] while mannose-containing oligosaccharides improve gut dysbiosis and intestinal barrier damage.[27]

As for the lipid A portion, this resulted in a complex blend of mono-phosphorylated tetra- and penta-acylated lipid A species carrying linear and branched acyl chains. Analogously, other *Bacteroides* and *Prevotella* species, all belonging to the phylum *Bacteroidota*, like *O. splanchnicus*, have been found to carry penta-acylated and mono-phosphorylated lipid A (Fig. 4).[29,31–35] Genomic analyses suggested that many *Bacteroidota* lack the enzymatic machinery required for the synthesis of more pro-inflammatory hexa-acylated lipid A species.[36] These observations support the notion that *O. splanchnicus* conforms to a broader structural paradigm of under-acylated, less inflammatory lipid A within the *Bacteroidota* phylum. In this frame, of particular interest for further investigation is the carbohydrate portion (Fig. 4), whose structural heterogeneity and peculiarities warrant deeper exploration from a biosynthetic standpoint.

Given the structural peculiarity of this LOS, we then investigated the supramolecular organization of the *O. splanchnicus* LOS, which is known to critically influence immunogenicity. Small Angle X-ray scattering measurements on the *O. splanchnicus* LOS unambiguously reveal its propensity to form monodisperse, spherical micelles in aqueous solution,

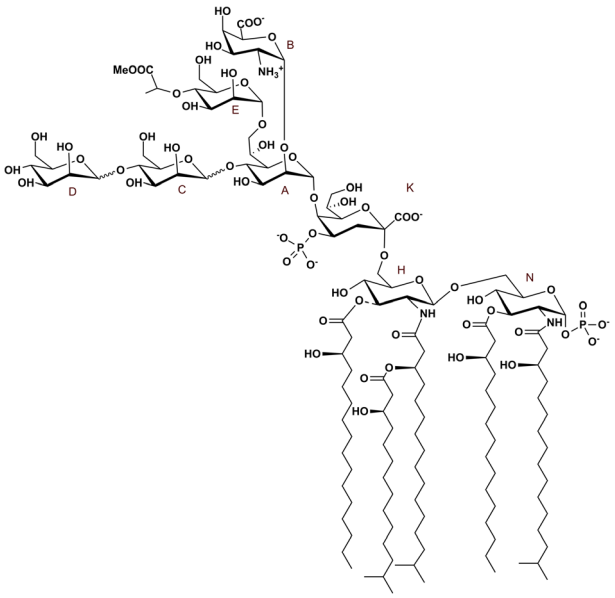

Fig. 4 Full structure of the LOS from *O. splanchnicus*. Branched fatty acids are represented in their iso-form; however they can also be found as linear or anteiso chains.

a supramolecular organization that mirrors self-assembly behavior reported for a broad range of bacterial LPSs/LOSs extracted from several bacterial strains.[37] As shown in Fig. 5, the experimental data were fitted using a core–shell model (eqn (1)), which effectively describes a spherical micelle composed of a compact hydrophobic core (Lipid A domains) surrounded by a hydrophilic shell.[38] The nonlinear least-squares fitting of the model yielded a hydrophobic core radius of 16.1 ± 0.1 Å and a total particle radius of 80.5 ± 0.4 Å. This aggregation state is essential, as it is known to influence how a LPS is recognized by the host immune system.[39] In particular, the extended oligosaccharide shell (~64 Å) sterically shields the lipid A moiety and limits access to the TLR4/MD-2 receptor complex. Such a "structural masking" mechanism has been shown to attenuate LPS immunostimulatory potential.[40] Taken together, the unique structural and aggregation properties of the *O. splanchnicus* LOS ensure its processing in a low-inflammatory manner. This may allow the bacterium to evade immune detection and preserve epithelial integrity, thus favoring the persistence of beneficial

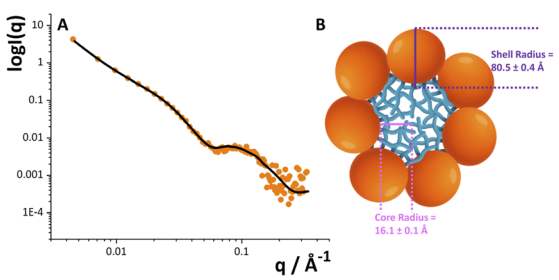

Fig. 5 (A) SAXS experimental data and best fit for the *O. splanchnicus* LOS in water. (B) Schematic depiction of the spherical micelle, showing the hydrophobic lipid A core (light blue) enveloped by the oligosaccharide shell (orange).

commensals in the gut and protecting against colonization by proinflammatory pathobionts.

Microarray studies

Lectin recognition of the *O. splanchnicus* LOS was examined in binding assays to the microarray-printed LOS.[41] First, the binding of a panel of 40 model lectins with diverse carbohydrate-binding specificities (Table S2) was tested. As shown in Fig. 6 (upper panel), negligible or very weak signals were detected for most lectins, including those exhibiting specificity for Man-containing structures, although lectin binding to the appropriate control glycoproteins was observed. This behavior indicates that Man residues are not in the appropriate configuration for recognition, as can be anticipated for 4-substituted Man. Significant signals were only detected for a limited number of lectins with nominal specificity for GlcNAc, Gal, or Fuc, which can be ascribed to peculiar features of their fine specificities. In addition, the binding of 17 human innate immune lectins (Table S3) was examined (Fig. 6, lower panel). Intense binding signals were observed for galectin-4, ficolins 2 and 3, intelectin-1, and mindin, as similarly observed for the LPS of *Paenalcaligenes hominis*.[42] The complexity of the *O. splanchnicus* LOS interactome with innate immune lectins is further expanded by collectin-11, which gave strong binding signals, and the other galectins tested, *i.e.* galectins 3, 7, 8, and 9, for which weak to moderate signals were detected. Besides calcium-dependent sugar recognition (Table S2), collectin-11 has been shown to bind DNA from diverse origins in a charge-dependent mode and it has been suggested to interact directly with several microbes in a calcium- and charge-dependent manner.[43]

Therefore, it is plausible that charge-mediated interactions could contribute to collectin-11's behavior, possibly owing to a suitable negative charge distribution in the LOS molecule. Regarding galectins, binding of galectin-3 to galacturonic acid in an unconventional orientation, flipped about 180° relative to the canonical binding mode, has been described,[44] raising the possibility that it could also accommodate a GalNA residue within the binding site. To the best of our knowledge, no similar studies have been reported for other galectins. These results encourage further in-depth analyses of the peculiar motifs of this LOS and their recognition by the innate immune lectins tested here.

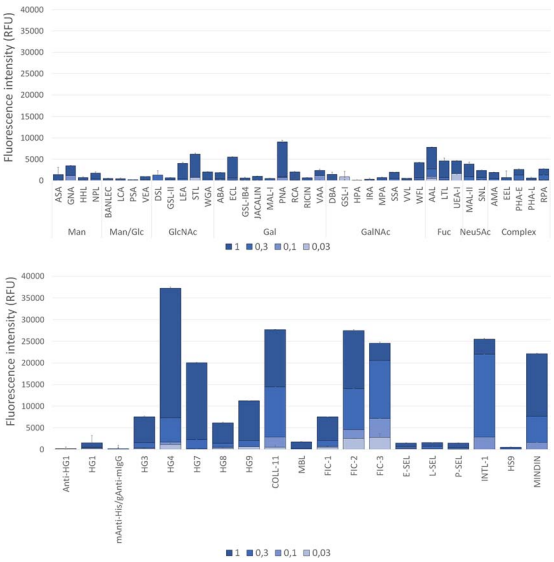

Fig. 6 Lectin binding to the microarray-printed *O. splanchnicus* LOS. The samples were printed as duplicates at different concentrations and the binding of two different collections of lectins was assayed, using AF647-streptavidin for final detection. Upper panel: binding of biotin-labelled model lectins with diverse carbohydrate-binding specificities (see Table S2). Lower panel: binding of innate immune lectins (see Table S3). Blank experiments, in the absence of lectins, with biotinylated rabbit anti-human galectin 1 antibody and with mouse anti-His antibody pre-complexed with biotinylated goat anti-mouse IgG antibody (see Materials and methods) were run in parallel. Data shown correspond to the mean of the fluorescence signals obtained for samples printed at 1, 0.3, 0.1, and 0.03 mg mL^{-1} (depicted in the dark to light blue color scale) and error bars indicate the standard deviation of the mean. HG, human galectin; COLL, collectin; MBL, mannan binding lectin; FIC, ficolin; SEL, selectin; INTL, intelectin; HS, human Siglec.

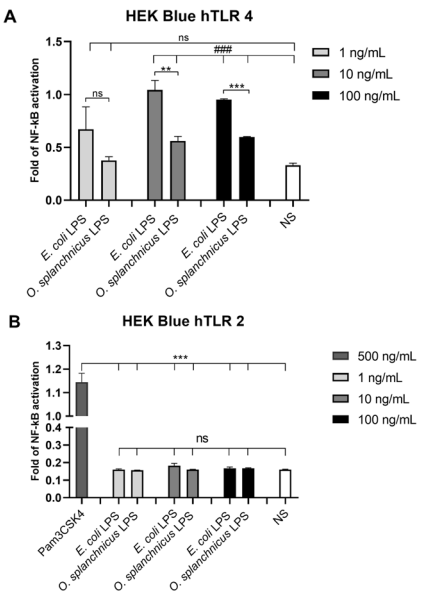

Fig. 7 Assessment of TLR activation by the *O. splanchnicus* LOS. (A) Stimulation of HEK Blue™ hTLR4 and (B) HEK Blue™ hTLR2 reporter cells. Secreted embryonic alkaline phosphatase (SEAP) levels (OD) measured upon exposure to the *E. coli* LPS or *O. splanchnicus* LOS at 1, 10, and 100 ng mL^{-1}. In (A), ultra-pure LPSs from *E. coli* O111:B4 served as the positive control being a potent TLR4 agonist, while in (B) it functioned as a negative control given its inability for TLR2 stimulation. For TLR2 activation in (B), Pam3CSK4 (500 ng mL^{-1}), a synthetic triacylated lipopeptide, was employed as the positive control, as an agonist for TLR2 signaling In (A), statistical comparisons are shown between the *O. splanchnicus* LOS and *E. coli* LPS (***p < 0.001; **p < 0.01; ns = not significant) and between each treatment and the unstimulated cells (NS) (###p < 0.001; ns = not significant). In (B), statistical comparisons are shown between the *O. splanchnicus* LOS, *E. coli* LPS, and untreated cells *versus* the positive control Pam3CSK4 (***p < 0.001); no significant differences were observed between the *O. splanchnicus* LOS, *E. coli* LPS, and the unstimulated cells (NS). Statistical significance was determined by the unpaired t-test. Data are presented as mean ± SD of three independent replicates.

O. splanchnicus LOS-mediated TLR activation

To assess the immunological properties of the *O. splanchnicus* LOS, different concentrations of the purified LOS were tested in HEK-Blue™ cells transfected with human TLR4, MD-2, and CD14 genes or HEK-Blue™ hTLR2 cells. The *O. splanchnicus* LOS exhibited a significantly weaker capability to activate TLR4 signaling compared to the pro-inflammatory *E. coli* LPS used as a positive control (10 and 100 ng, ***$p < 0.001$, Fig. 7A). In parallel, no significant activation compared to untreated cells was observed in HEK-Blue™ hTLR2, indicating that the *O. splanchnicus* LOS is unable to activate TLR2 signaling (Fig. 7B).

O. splanchnicus LOS impact on enterocytes

The *O. splanchnicus* LOS was tested in the enterocyte cell line HT-29 and clearly showed no induction of IL-8 release as the level of the proinflammatory cytokine in the supernatant was similar to the cell medium serving as the background control (Fig. 8).

In accordance, the amount of IL-8 released was also significantly lower than IL-8 levels induced by the corresponding concentrations of the different *E. coli* LPSs used (B5, B6, and B8). In addition, we also evaluated whether the *O. splanchnicus* LOS was able to compete with proinflammatory *E. coli* LPSs in the HT-29 cell model. Interestingly, we observed that this peculiar LOS could compete with all three inflammatory *E. coli* LPSs with a ratio of 1 : 1 and 1 : 10, and significantly decreased IL-8 release compared to cells only induced by *E. coli* LPSs (Fig. 9A). The effect was even more profound when the ratio of *O. splanchnicus* LOSs was 10 times higher than proinflammatory LPSs. Finally, in a parallel experiment we first primed HT-29 cells with the *O. splanchnicus* LOS and, only after its removal, cells were treated with the *E. coli* LPS. Also in this case, we observed a decrease in the IL-8 release as compared to the control, *i.e.* attenuation of the *E. coli* LPS effect (ratios of 1 : 1 and 10 : 1, Fig. 9B). These observations are extremely interesting considering that *O. splanchnicus* cells and OMVs exert anti-inflammatory effects by attenuating *E. coli* LPS-induced IL-8 release from enterocytes, although the responsible effector molecules were not identified thus far.[4] The present study now points to the LOS of *O. splanchnicus* as a key mediator of this effect and establishes a link between its anti-inflammatory properties and distinct structural features of both the lipid A and core oligosaccharide domains.

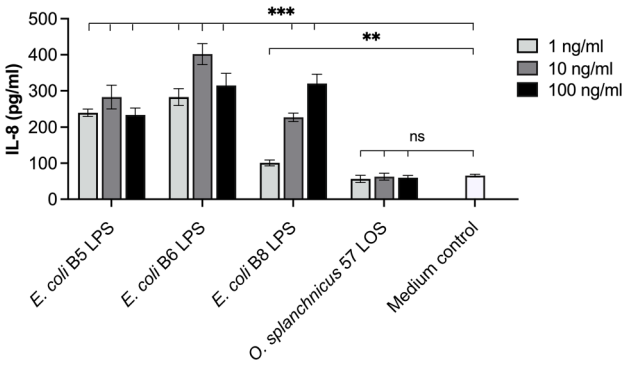

Fig. 8 Induction of IL-8 release from HT-29 cells by commercial *E. coli* LPSs (B5, B6 and B8) and *O. splanchnicus* isolate 57 LOS. The HT-29 cell medium (McCoy 5A) was used as a control. Representative results are shown as a mean and standard deviation of three technical replicates. * = $p < 0.05$, ** = $p < 0.01$, *** = $p < 0.001$, ns = not significant.

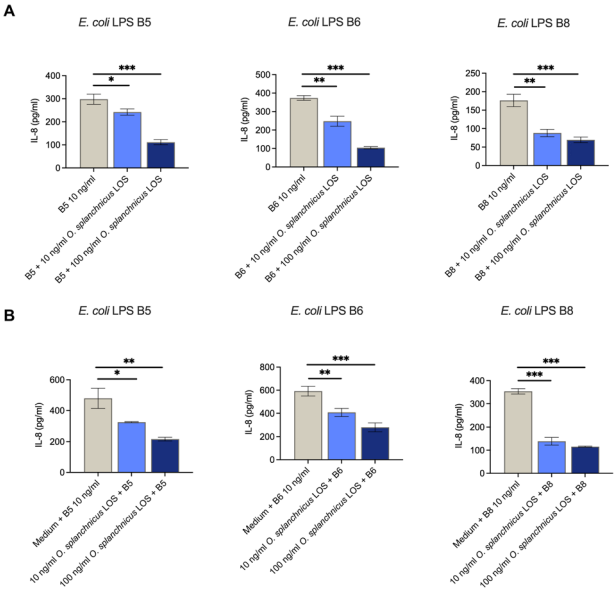

Fig. 9 (A) Competition of the *O. splanchnicus* LOS and *E. coli* LPS (B5, B6 and B8) in the induction of IL-8 release from HT-29 cells. The *E. coli* LPS alone (10 ng mL^{-1}) was used as a control. (B) Attenuation of the *E. coli* LPS induced IL-8 release from HT-29 cells by the *O. splanchnicus* LOS. The HT-29 medium alone followed by 10 ng mL^{-1} *E. coli* LPS was used as a baseline. Representative results (A and B) are shown as a mean and standard deviation of three technical replicates. * = $p < 0.05$, ** = $p < 0.01$, *** = $p < 0.001$, ns = not significant.

Conclusions

The use of commensal gut bacteria as "next-generation probiotics" may offer greater benefits compared to traditional probiotic formulations. These benefits may include improved retention in the gastrointestinal environment, enhanced adhesion to intestinal epithelial tissues, potent immunomodulatory effects, and the production of unique beneficial metabolites not typically associated with conventional probiotics.[45] Among the gut commensals that meet these criteria is *O. splanchnicus*, with potential applications in the prevention or management of metabolic and inflammatory diseases.[46,47] Indeed, although many aspects of its metabolic pathways and general biological functions remain largely unknown, evidence suggests that elevated levels of *O. splanchnicus* are positively associated with a healthy gastrointestinal status.[9] The results of this study highlight the *O. splanchnicus* LOS as a structurally and functionally distinct bacterial glycolipid with important implications for host–microbe interactions. Our combined structural, biophysical, and functional analyses reveal a lipid A architecture consistent with the broader *Bacteroidota* paradigm of hypoacylated, mono-phosphorylated species with intrinsically

reduced proinflammatory potential, in contrast to the canonical hexa-acylated lipid A of enterobacteria. The core OS further introduces rare and immunologically relevant motifs, including GalNA and the unprecedented incorporation of D-Man4Lac in the *Bacteroidota* phylum, both of which are plausibly linked to unique lectin recognition and to immunomodulation. The observed structural heterogeneity, together with selective binding to innate immune lectins, such as galectin-4, ficolins, and collectin-11, underscore the potential of this LOS to engage host immunity through non-canonical pathways.[13] Importantly, the supramolecular organization of the *O. splanchnicus* LOS into micelles with an extended oligosaccharide shell provides a mechanistic explanation for its weak TLR4 activation and its antagonism of proinflammatory *E. coli* LPS signaling. These features converge to create a low-inflammatory phenotype that facilitates immune tolerance, epithelial integrity, and the commensal persistence of *O. splanchnicus*. Although the exact micellar architecture may not be preserved in the complex milieu of the gut, the SAXS data capture the intrinsic self-assembly propensity of this LOS and reveal a structural arrangement in which the oligosaccharide domain effectively limits exposure of the lipid A region. This inherent steric attenuation of lipid A accessibility, together with its hypo-acylated and hypo-phosphorylated nature, are likely the main factors underlying its reduced TLR4 recognition *in vivo*.

By linking distinctive glycan motifs and aggregation states to biological outcomes, this work establishes the LOS of *O. splanchnicus* as a key determinant of its beneficial immunomodulatory effects, reinforcing the potential of this species as a next-generation probiotic candidate.

Experimental

O. splanchnicus isolation

O. splanchnicus isolate 57 was isolated, purified and identified from the feces of an FMT (fecal microbiota transplant) donor in our previous study.[5] The donor provided written informed consent, and the use of the sample was approved by the Ethics Committee of Hospital District of Helsinki and Uusimaa Finland (DnroHUS124/13/03/01/11). The *O. splanchnicus* isolate was cultivated on Gifu anaerobic medium (GAM; Nissui Pharmaceutical Co., Ltd, Japan) for 48 h under anaerobic conditions at 37 °C in an anaerobic chamber (Whitley 85A anaerobic workstation).[36] The isolate was genome sequenced using the MiSeq (Illumina, Inc., San Diego, CA, United States; BioProject PRJNA575760). The bacterium was preserved as frozen stocks in skim milk tubes at −80 °C. For the LOS extraction, *O. splanchnicus* was propagated from a frozen stock on a GAM agar plate and grown for 48 h anaerobically. After confirming the purity of the isolate, 2 L culture of *O. splanchnicus* isolate 57 was grown in GAM broth for 48 h followed by pelleting the cells (4700 rpm, 10 min).

Isolation and purification of the LOS from *O. splanchnicus*

The dried bacterial cells (1 g) were extracted with the hot phenol-water protocol.[48] The obtained aqueous and phenolic phases were further dialyzed and subjected to enzymatic digestion with DNase (Sigma-Aldrich, Darmstadt, Germany) and RNase (Sigma-Aldrich, Darmstadt, Germany) followed by proteinase K (Sigma-Aldrich, Darmstadt, Germany) (37 and 56 °C). The purity and nature of the extracted material (111 mg) was checked *via* SDS-PAGE stained with silver nitrate gel (Fig. S1).[49]

Chemical analyses

To determine the monosaccharide composition, the acetylated *O*-methyl glycoside derivative method was used, and the treatment starts with HCl/MeOH (1.25 M, 358 K, 12 h) followed by acetylation with acetic anhydride in pyridine (358 K, 30 min).[50] To determine the absolute configuration of the sugars, *O*-octylglycoside derivatives were prepared and analyzed as previously described.[51] The sugar linkage pattern was determined with an aliquot of LOS suspended in DMSO in the presence of NaOH, stirred at room temperature for 1.5 h. Then, the methylation step was achieved with CH_3I, followed by hydrolysis with trifluoroacetic acid (4 M, 373 K, 4 h), a reduction of the carbonyl with $NaBD_4$ and acetylation with pyridine and acetic anhydride. In parallel, in order to analyze the fatty acids present in the sample, another LOS aliquot underwent the previously described methanolysis step and then the mixture was extracted three times with hexane. Hexane which contained the fatty acids was analyzed *via* GC-MS. All chemical analyses were carried out on a gas-chromatograph Agilent Technologies 6850A (Santa Clara, CA, USA) equipped with a mass selective detector 5973N and a Zebron ZB-5 capillary column (Phenomenex, 30 m × 0.25 mm i.d., 0.25 μm film thickness, flow rate 1 mL min^{-1}, he as the carrier gas). The temperature program 413 K for 5 min, 413 K → 553 K at 10 °C min^{-1}, and 553 K for 10 min was used for lipid analysis, and for sugar analysis the temperature program was 423 K for 5 min, 423 K → 553 K at 3 °C min^{-1}, and 553 K for 5 min.

Isolation of the OS_{deAc}, OS and lipid A fractions

An aliquot of LOS (30 mg) was subjected to *O*-deacylation with anhydrous hydrazine (1 mL, at 310 K for 90 min), and the suspension created was cooled and transferred into ice-cold acetone to allow precipitation. The precipitate was centrifuged (277 K, 5000×*g*, 30 min) and washed again with ice-cold acetone, dried, dissolved in water and then freeze-dried. The *O*-deacylated product obtained underwent *N*-deacylation with 4 M KOH (393 K, 16 h) resulting in the OS_{deAc} product. The salts resulting from the reactions were eliminated using gel-filtration chromatography on a Sephadex G-10 column (Pharmacia, 50 × 1.5 cm). In parallel, another aliquot (9 mg) was treated with acetic acid at 1% (373 K, 2 h) in order to separate the lipid A from the core OS portion. The solution was extracted three times with a mixture of $CHCl_3$/MeOH/H_20 (100 : 30 : 30, v/v/v) and then centrifuged (277 K, 7000×*g*, 15 min). The organic phase contained lipid A and was washed three times with distilled water and freeze-dried to obtain the isolated lipid A product. The aqueous phase contained the product and was also collected and freeze-dried for further analysis. At this point, first, gel filtration chromatography (TSK40) and then high-

performance gel permeation chromatography (HPGPC) on a TSKgel G3000 PWXL column were performed.

NMR spectroscopy

To assign the structure of the oligosaccharide, the NMR spectra were recorded in D_2O at 298 K at pH 7 with a Bruker 600 AVANCE NEO equipped with a cryoprobe. Total correlation spectroscopy (TOCSY) experiments were performed with spin-lock times of 100 ms and a data set ($t_1 \times t_2$) of 4096 × 512 points. The Rotating-frame Overhauser enhancement spectroscopy (ROESY) and nuclear Overhauser enhancement spectroscopy (NOESY) measurements were performed with data sets ($t_1 \times t_2$) of 4096 × 512 points and mixing times ranging from 100 to 400 ms. Double-quantum-filtered phase-sensitive correlation spectroscopy (DQF-COSY) experiments were conducted using data sets of 4096 × 912 points. To give a 4 K × 2 K point matrix, the data matrix of all homonuclear experiments was filled with zeros in both dimensions. Afterwards, the resolution enhancement was used in the dimensions *via* a cosinebell function prior to Fourier transformation. To obtain the coupling constant, 2D phase-sensitive DQF-COSY measurements were used. Heteronuclear single-quantum coherence (HSQC) and heteronuclear multiple–bond correlation (HMBC) experiments were carried out in the ^{1}H-detection mode using single-quantum coherence with proton decoupling in the ^{13}C domain using data sets of 2048 × 400 points. Phase-sensitive mode and sensitivity improvements were applied for HSQC, along with echo/antiecho gradient selection and multiplicity editing in the selection step. In the HMBC experiments, an optimization was applied for long-range coupling constants, incorporating a low-pass *J* filter to eliminate the one-bod correlations, *via* gradient pulses for selection. Furthermore, a 60 ms delay was used for the evolution of long-range correlations, with an optimization for 6–15 Hz coupling constants. To improve resolution, the data matrix in the heteronuclear experiment was extended to 2048 × 1024 points with forward linear prediction extrapolation.

ESI MS and MS/MS analyses

OS_{deAc} was dissolved in a solution composed of 50% (v/v) methanol and 50% water and directly infused by using a syringe pump (10 μL min^{-1}, at an estimated concentration of 10 μg mL^{-1}) into the source of a Waters Synapt XS mass spectrometer, equipped with an 8 kDa quadrupole with an electrospray ionization (ESI) source. The analysis was conducted with a capillary potential of −2.00 kV, source temperature of 120 °C, sampling cone at 20.0 V, source offset at 0 V, source gas (N_2) flow of 0.0 mL min^{-1}, desolvation temperature of 400 °C, cone gas flow of 20 L h^{-1}, desolvation gas flow of 150 L h^{-1}, and nebulizer gas pressure of 2.5 bar. An aliquot of LOS was dissolved in 400 μL of a 1 M aqueous solution of ammonia (NH_3). The solution was stirred overnight at 37 °C. Then, the solution was dried under air flow, followed by freeze-drying to obtain the *O*-deacylated LOS. This product was dissolved in 50% (v/v) 2-propanol and 50% water and directly infused by using a syringe pump (5 μL min^{-1}, at an estimated concentration of 20 μg mL^{-1}). The analysis was carried out with a capillary potential of −1.9 kV, source temperature of 120 °C, sampling cone at 40.0 V, source offset at 10 V, source gas (N_2) flow of 0.0 mL min^{-1}, desolvation temperature of 400 °C, cone gas flow of 60 L h^{-1}, desolvation gas flow of 300 L h^{-1}, and nebulizer gas pressure of 2.5 bar. All the analyses were performed in negative polarity and resolution mode with a scan range between *m*/*z* 50 and *m*/*z* 2000 and a scan time of 1 s. Nitrogen was supplied by a PLINIUS N45-1 nitrogen generator from CLAIND and was used as desolvation and cone gas. MS/MS experiments were performed using ultrapure argon (SOL SpA) as the collision gas in the trap cell, with a collision energy ramp ranging from 20 to 90 eV. A 2 μg μL^{-1} solution of NaI in (v/v) 2-propanol/H_2O 50 : 50 was used for the calibration from 50 to 4000 Da. Data acquisition and MS and MS/MS spectral images were generated by MassLynx™ software (V4.2).[52] A reference solution consisting of 100 pg μL^{-1} Leucine Enkephalin dissolved in a 1 : 1 (vol/vol) mixture of water/acetonitrile with 0.1% of formic acid was used as lockmass during sample acquisition with a lockspray capillary of −2.5 kV and a scan time of 0.5 s.

MALDI-TOF MS analysis

MALDI-TOF MS spectra were obtained using an ABSCIEX TOF/TOFTM 5800 mass spectrometer from Applied Biosystems, equipped with an Nd:YAG laser (wavelength of 349 nm), featuring a pulse width of 3 ns and a maximum repetition rate of 1000 Hz. The lipid A fraction was dissolved in $CHCl_3$/CH_3OH (1 : 1, v/v) while the matrix was 2,4,6-trihydroxyacetophenone in CH_3OH/0.1% trifluoroacetic acid/CH_3CN (7 : 2 : 1, v/v) at a concentration of 75 mg mL^{-1}.[53,54] 0.5 μL of both the sample and the matrix were deposited on the MALDI plate and allowed to dry at ambient temperature. Each spectrum represented an accumulation of 2000 laser shots, while the MS/MS spectra involved the summation of between 5000 and 7000 shots. Acquisition was performed ensuring random yet uniform sampling across the sample spot.

HEK cell culture and stimulation assays

HEK-Blue hTLR4 and HEK-Blue hTLR2 were provided by Invivogen (Invivogen, Toulouse, France) and cultured in Dulbecco's Modified Eagle's Medium (DMEM) 4 g L^{-1} glucose supplemented with 10% heat-inactivated fetal bovine serum (FBS), 1% penicillin/streptomycin (pen/strep), 2 mM L-glutamine and 100 μg mL^{-1} Normocin. To ensure plasmid selection, HEK-Blue selection was added to HEK-Blue cell culture medium according to the manufacturer's instructions. Cell lines were maintained at 37 °C in a humidified atmosphere containing 5% CO_2. HEK-Blue hTLR4 and HEK-Blue hTLR2 were seeded into a 96-well plate (3 × 104 cells per well). After an overnight attachment, HEK-Blue cells were stimulated for 18 hours with various concentrations of *E. coli* O111:B4 LPS (Invivogen, Toulouse, France) or *O. splanchnicus* LOS. NF-kB activation was measured by Quanti blue assay (Invivogen, Toulouse, France). HEK-Blue hTLR2 cells were also treated with 500 ng mL^{-1} Pam3CSK4 (Invivogen, Toulouse, France), a positive control for TLR2 activation. The secreted embryonic alkaline phosphatase

(SEAP) levels were evaluated in the supernatants to establish NF-kB activation following LPS stimulation by Quanti-Blue assay. For this assay, the absorbance at 620 nm was measured by using a TECAN Infinite M Plex spectrophotometer (Tecan, Grödig, Austria).

HT-29 cell line

The human colonic epithelial cell line HT-29 (ACC 299) was purchased from the German Collection of Microorganisms and Cell Cultures (DSMZ). The cell line was grown under an oxic atmosphere with 5% CO_2 at 37 °C. HT-29 cells were cultivated in McCoy 5A (Biowest) medium containing 10% heat-inactivated fetal bovine serum (FBS; Gibco) and 100 U mL^{-1} penicillin/streptomycin solution (PEST). The cells were passaged after reaching 80% confluence (every 3–4 days) using TryplExpress (Gibco) to detach the cells. Passages 6–20 were used in the experiments. For the immunological assays, 12.500 HT-29 cells per well were seeded onto a 96-well microplate and grown for 8 days post-plating under an oxic atmosphere with 5% CO_2 at 37 °C. The medium in the wells was changed every 3–4 days and one day before the experiment. The confluence of HT-29 cells in each well was checked before the assay. Three different commercial *E. coli* LPSs were purchased from Merck. LPSs from strains DSM4779 O55:K59(B5), ATCC 12795 O26(B6) and O127:(B8) were used in the experiments.

IL-8 release from HT-29: induction, competition & attenuation

The capacity of the *O. splanchnicus* 57 LOS to induce IL-8 release from HT-29 cells was measured as previously described.[5] Three different commercial *E. coli* LPSs were used in comparison. In the induction assay, 1 ng mL^{-1}, 10 ng mL^{-1} and 100 ng mL^{-1} of LOS were suspended in McCoy 5A medium, added onto 8-day-old HT-29 cells and incubated at 37 °C for 3 h under an oxic atmosphere with 5% CO_2. The McCoy 5A medium without LPSs was used as the background control. Supernatants were collected and IL-8 levels were measured by using an ELISA assay (BD OptEIA Set).

In the competition assay, 10 ng mL^{-1} of proinflammatory *E. coli* LPS was used in the HT-29 cell experiments. Briefly, the *O. splanchnicus* LOS was mixed with different ratios 1 : 1 (10 ng mL^{-1} *E. coli* LPS + 10 ng mL^{-1} *O. splanchnicus* 57 LOS) or 1 : 10 (10 ng mL^{-1} *E. coli* LPS + 100 ng mL^{-1} *O. splanchnicus* 57 LOS) and incubated on an 8-day old, fully confluent HT-29 monolayer for 3 h before collecting the supernatants for ELISA IL-8 measurement. *E. coli* LPS 10 ng mL^{-1} was used as the baseline control.

In the attenuation assay, HT-29 cells were first incubated with the *O. splanchnicus* LOS for 1 h with a concentration of either 10 ng mL^{-1} or 100 ng mL^{-1}. After removing the *O. splanchnicus* LOS from the monolayer, the proinflammatory *E. coli* LPS (10 ng mL^{-1}) was added onto the cells for 4 h followed by collection of the supernatants and IL-8 measurements with ELISA.

Statistical analysis

Significant differences between two groups, for example the sample and control, were calculated using an unpaired *t*-test. Homoscedasticity testing was carried out with Levene's test to identify equal or unequal variances. All statistical analyses were calculated with GraphPad Prism 10.5.0 (GraphPad Software, United States). A *p*-value of <0.05 was considered statistically significant.

Small Angle X-ray scattering (SAXS)

Small-angle X-ray scattering (SAXS) was employed to probe the self-assembly behavior of lipooligosaccharide (LOS) in an aqueous suspension. Measurements were conducted on the Diamond Light Source B21 beamline (Didcot, UK), operating at an X-ray energy of 13.018 keV and a sample-to-detector distance of 3.7 m. Using this configuration, it was possible to collect data for the scattering vector modulus $Q = 4\pi\sin(\theta/2)\ \lambda$ between 0.0045 $Å^{-1}$ and 0.34 $Å^{-1}$, where θ is the scattering angle.[55–57]

The SAXS experimental data in the present work were fitted with the SASView v 5.0.6 Software (https://www.sasview.org/) using a core–shell sphere model:

$$P(q) = \frac{\text{scale}}{V}F^2(q) + \text{background} \quad (1)$$

where:

$$F(q) = \frac{3}{V_s}\left[V_c(\rho_c - \rho_s)\frac{\sin(qr_c) - qr_c\cos(qr_c)}{(qr_c)^3} + V_s(\rho_s - \rho_{solv})\frac{\sin(qr_s) - qr_s\cos(qr_s)}{(qr_s)^3}\right] \quad (2)$$

where V_s is the volume of the whole particle, V_c is the volume of the core, r_s = radius + thickness is the radius of the particle, r_c is the radius of the core, ρ_c is the scattering length density of the core, ρ_s is the scattering length density of the shell, and ρ_{solv} is the scattering length density of the solvent.

Microarray binding assays

The *O. splanchnicus* LOS and control (glyco)proteins (asialofetuin, ribonuclease B, and ribonuclease A) were printed as duplicates at four different concentrations (from 1 to 0.03 mg mL^{-1}) on 16-pad nitrocellulose-coated glass slides (Grace Bio-labs ONCYTE NOVA) using a non-contact arrayer (Sprint, Arrayjet Ltd), as described.[41] The Cy3 fluorophore (GE Healthcare) was added at 1 μg mL^{-1} to all the solutions to enable postarray monitoring of the spots[58] by using scanning fluorescence signals upon excitation at 532 nm (green laser), using a GenePix 4200-AL scanner (Axon, Molecular Devices). For binding assays, the microarrays were first blocked for 1 h with 0.25% (v/v) Tween-20 in 5 mM sodium phosphate, pH 7.2, 0.2 M NaCl (PBS) or in 10 mM Tris pH 8, 150 mM NaCl (TBS). Then, the arrays were overlaid for 1.5 h with biotin-labelled lectins at 10 μg mL^{-1} in an appropriate buffer containing 0.1% (v/v) Tween-20. A panel of 40 lectins was assayed (see Table S2 for details on lectins tested, source, and buffer used in each case). Similarly, for testing the binding of human innate immune

lectins, the arrays were overlaid with the lectins at 20 μg mL^{-1} (tags, source of the lectins tested, and buffers used are listed in Table S3). After incubation and subsequent washing steps, pads were incubated for 1 h with either biotinylated rabbit anti-human galectin 1 (Peprotech, working dilution 1 : 1000) or mouse anti-His antibody pre-complexed with biotinylated goat anti-mouse IgG antibody (Sigma, final working dilutions 1 : 1000 and 3 : 1000, respectively). The slides were washed 4 times with PBS and binding was detected by incubating with AlexaFluor-647 (AF647)-labelled streptavidin (invitrogen) at 1 μg mL^{-1} in PBS or TBS, 0.1% (v/v) Tween-20, for 35 min in the dark, washed again thoroughly with PBS, then with water and finally scanned for AF647 signals (excitation at 635 nm, red laser). Fluorescence intensities were quantified with the GenePix Pro 7 software.

Author contributions

A. S. conceived the study; M. T. M. executed the LOS isolation purification, and characterization; F. D. L and M. M executed the MRM/MS studies; R. S. and K. H. provided the bacterial strain and studied the impact on enterocytes; L. D. S. C performed HEK cell assays; M. A. C. R. and D. S. executed the microarray binding essays; A. C. and L. P. executed small angle X-ray scattering; funding and resource acquisition: A. S., F. D. L., A. M. and R. S; writing – original draft preparation: M. T. M., M. M., and K. H.; writing – review and editing: A. S., F. D. L., A. M., D. S. and R. S. All authors have read and have given approval to the final version of the manuscript.

Conflicts of interest

There are no conflicts to declare.

Data availability

The data supporting this article have been included as part of the supplementary information (SI). Supplementary information: SI reports Fig. S1–S3 with SDS-PAGE, NMR and MS data, as well as Tables S1–S3 with NMR and microarray data. See DOI: https://doi.org/10.1039/d5sc08335d.

Acknowledgements

The authors wish to thank the Diamond Light Source for providing beamtime (reference SM34244-1). This work was supported by the European Research Council (ERC) under the Horizon Europe program under grant agreement no. 101039841 (DEBUGGING LPS) to F. D. L. This work has also received funding from the European Union's Horizon Europe research and innovation programme under grant agreement no. 101095084 for the ENDOTARGET project, which is also supported by the Swiss State Secretariat for Education, Research and Innovation (SERI) under contract number 22.00462. It was also supported by the project "CLariFY" and "GIVING" funded by the Italian Ministry of University and Research, PRIN MUR 2022 (2022SHW3KY) and PRIN MUR PNRR 2022 (P202293ZMC) to F. D. L. MAC-R and DS were funded by grant PID2022-143249OB-I00 of MCIN/AEI/10.13039/501100011033 and "ERDF A way of making Europe", and by CIBER (Consorcio Centro de Investigación Biomédica en Red (CIBERES), Instituto de Salud Carlos III), CB06/06/0037. This work was also supported in part by the Italian Ministry of Foreign Affairs and International Cooperation (Italy Germany Science and Technology cooperation–Call for joint research proposals for the years 2023–2025). This research was funded under the National Recovery and Resilience Plan (NRRP), Mission 4 Component 2 Investment 1.3—Call for tender no. 341 of 15 March 2022 of Italian Ministry of University and Research funded by the European Union—NextGenerationEU. Project code PE00000003, Concession Decree no. 1550 of 11 October 2022, adopted by the Italian Ministry of University and Research, CUP E63C22002030007, Project title "ON Foods—Research and innovation network on food and nutrition Sustainability, Safety and Security—Working ON Foods". H2020-MSCA-ITN-2020, contract no. 956758 (AS, MTM). Ministry of Education, Universities and Research, PRIN MUR 2022 (2022ZEZS45) and Ministry of Education, Universities and Research, PRIN MUR PNRR 2022 (P2022M457Z) (AS). PNRR, Missione 4 – Componente 2 – NextGenerationEU – Partenariato Esteso INF-ACT – One Health Basic and Translational Research Actions Addressing Unmet Needs on Emerging Infectious Diseases MUR: PE00000007 (AS).

References

1 I. Schoultz, M. J. Claesson, M. G. Dominguez-Bello, F. Fåk Hållenius, P. Konturek, K. Korpela, M. F. Laursen, J. Penders, H. Roager, T. Vatanen, L. Öhman and M. C. Jenmalm, *J. Intern. Med.*, 2025, **297**, 560–583.
2 M. Göker, S. Gronow, A. Zeytun, M. Nolan, S. Lucas, A. Lapidus, N. Hammon, S. Deshpande, J. F. Cheng, S. Pitluck, K. Liolios, I. Pagani, N. Ivanova, K. Mavromatis, G. Ovchinikova, A. Pati, R. Tapia, C. Han, L. Goodwin, A. Chen, K. Palaniappan, M. Land, L. Hauser, C. D. Jeffries, E. M. Brambilla, M. Rohde, J. C. Detter, T. Woyke, J. Bristow, V. Markowitz, P. Hugenholtz, J. A. Eisen, N. C. Kyrpides and H. P. Klenk, *Stand. Genomic Sci.*, 2011, **4**, 200–209.
3 J. Li, J. Xu, X. Guo, H. Xu, C. Huang, Y. Nie and Y. Zhou, *Microorganisms*, 2025, **13**, 815.
4 J. D. Lewis, E. Z. Chen, R. N. Baldassano, A. R. Otley, A. M. Griffiths, D. Lee, K. Bittinger, A. Bailey, E. S. Friedman, C. Hoffmann, L. Albenberg, R. Sinha, C. Compher, E. Gilroy, L. Nessel, A. Grant, C. Chehoud, H. Li, G. D. Wu and F. D. Bushman, *Cell Host Microbe*, 2015, **18**, 489–500.
5 K. Hiippala, G. Barreto, C. Burrello, A. Diaz-Basabe, M. Suutarinen, V. Kainulainen, J. R. Bowers, D. Lemmer, D. M. Engelthaler, K. K. Eklund, F. Facciotti and R. Satokari, *Front. Microbiol.*, 2020, **11**, 575455.
6 J. Zhuang, Z. Zhuang, B. Chen, Y. Yang, H. Chen and G. Guan, *J. Mol. Med.*, 2025, **31**, 1–14.

7 D. G. Burke, F. Fouhy, M. J. Harrison, M. C. Rea, P. D. Cotter, O. O'Sullivan, C. Stanton, C. Hill, F. Shanahan, B. J. Plant and R. P. Ross, *BMC Microbiol.*, 2017, **17**, 1–11.
8 Q. Chen, Y. Fan, B. Zhang, C. Yan, Q. Zhang, Y. Ke, Z. Chen, L. Wang, H. Shi, Y. Hu, Q. Huang, J. Su, C. Xie, X. Zhang, L. Zhou, J. Ren and H. Xu, *Microbiol. Spectr.*, 2023, **11**, e04152.
9 S. F. Lima, L. Gogokhia, M. Viladomiu, L. Chou, G. Putzel, W. B. Jin, S. Pires, C. J. Guo, Y. Gerardin, C. V. Crawford, V. Jacob, E. Scherl, S. E. Brown, J. Hambor and R. S. Longman, *Gastroenterology*, 2022, **162**, 166–178.
10 B. S. Oh, W. J. Choi, J. S. Kim, S. W. Ryu, S. Y. Yu, J. S. Lee, S. H. Park, S. W. Kang, J. Lee, W. Y. Jung, Y. M. Kim, J. H. Jeong and J. H. Lee, *Front. Microbiol.*, 2021, **12**, 736343.
11 B. Bosch, S. Moutaharrik, A. Gazzaniga, K. Hiippala, H. A. Santos, A. Maroni and R. Satokari, *Eur. J. Pharm. Biopharm.*, 2023, **190**, 73–80.
12 F. Di Lorenzo, K. A. Duda, R. Lanzetta, A. Silipo, C. De Castro and A. Molinaro, *Chem. Rev.*, 2021, **122**, 15767–15821.
13 S. De Chiara, L. De Simone Carone, R. Cirella, E. Andretta, A. Silipo, A. Molinaro, M. Mercogliano and F. Di Lorenzo, *ChemMedChem*, 2025, **20**, e202400780.
14 B. S. Park and J. O. Lee, *Exp. Mol. Med.*, 2013, **45**, e66.
15 F. Bäckhed, S. Normark, E. K. H. Schweda, S. Oscarson and A. Richter-Dahlfors, *Microb. Infect.*, 2003, **5**, 1057–1063.
16 G. I. Birnbaum, R. Rene, J. R. Brisson and H. J. Jennings, *J. Carbohydr. Chem.*, 1987, **6**, 17–39.
17 R. Marchetti, R. E. Forgione, F. N. Fabregat, C. Di Carluccio, A. Molinaro and A. Silipo, *Curr. Opin. Struct. Biol.*, 2021, **68**, 74–83.
18 Y. A. Knirel, O. V. Bystrova, N. A. Kocharova, U. Zähringer and G. B. Pier, *J. Endotoxin Res.*, 2006, **12**, 324–336.
19 F. Sisti, J. Fernández, A. Cordero, A. Casabuono, A. Couto and D. Hozbor, *Bioorg. Med. Chem. Lett.*, 2017, **27**, 432–436.
20 D. Garozzo, G. Impallomeni, E. Spina, L. Sturiale, A. Cesàro and P. Cescutti, *Carbohydr. Res.*, 1995, **270**, 97–106.
21 N. K. Kochetkov, A. F. Sviridov, K. A. Arifkhodzhaev, O. S. Chizhov and A. S. Shashkov, *Carbohydr. Res.*, 1979, **71**, 193–203.
22 E. N. Sigida, I. M. Ibrahim, M. S. Kokoulin, H. H. Abulreesh, K. Elbanna, S. A. Konnova and Y. P. Fedonenko, *Mar. Drugs*, 2021, **19**, 508.
23 R. F. Helm, Z. Huang, D. Edwards, H. Leeson, W. Peery and M. Potts, *J. Bacteriol.*, 2000, **182**, 974–982.
24 H. Li, S. Liu, Y. Liu, W. Li, A. Niu, P. Ren, Y. Liu, C. Jiang, M. Inam and L. Guan, *Carbohydr. Polym.*, 2022, **281**, 119055.
25 Y. Yang, P. Ren, Y. Sun, J. Li, X. Zhou, H. Zhang, C. He, H. Dai and L. Guan, *Int. J. Biol. Macromol.*, 2024, **283**, 137435.
26 M. Dhanalakshmi, D. Sruthi, K. R. Jinuraj, K. Das, S. Dave, N. M. Andal and J. Das, *Med. Chem. Res.*, 2023, **32**, 391–408.
27 Y. Du, Y. Fan, X. Li and F. Chen, *npj Biofilms Microbiomes*, 2025, **11**, 1–22.
28 M. Tiemblo Martín, M. Coccimiglio, E. Andretta, L. De Simone Carone, A. Bell, T. Guerpe Amor, C. Di Carluccio, A. Molinaro, Y. van Kooyk, N. Juge, F. Chiodo, F. Di Lorenzo and A. Silipo, *Carbohydr. Polym.*, 2025, **348**, 122833.
29 M. D. Pither, A. Illiano, C. Pagliuca, A. Jacobson, G. Mantova, A. Stornaiuolo, R. Colicchio, M. Vitiello, G. Pinto, A. Silipo, M. A. Fischbach, P. Salvatore, A. Amoresano, A. Molinaro and F. Di Lorenzo, *Carbohydr. Polym.*, 2022, **297**, 120040.
30 F. Di Lorenzo, M. D. Pither, M. Martufi, I. Scarinci, J. Guzmán-Caldentey, E. Łakomiec, W. Jachymek, S. C. M. Bruijns, S. M. Santamaría, J. S. Frick, Y. Van Kooyk, F. Chiodo, A. Silipo, M. L. Bernardini and A. Molinaro, *ACS Cent. Sci.*, 2020, **6**, 1602–1616.
31 M. Hashimoto, Y. Asai, R. Tamai, T. Jinno, K. Umatani and T. Ogawa, *FEBS Lett.*, 2003, **543**, 98–102.
32 T. Vatanen, A. D. Kostic, E. D'Hennezel, H. Siljander, E. A. Franzosa, M. Yassour, R. Kolde, H. Vlamakis, T. D. Arthur, A. M. Hämäläinen, A. Peet, V. Tillmann, R. Uibo, S. Mokurov, N. Dorshakova, J. Ilonen, S. M. Virtanen, S. J. Szabo, J. A. Porter, H. Lähdesmäki, C. Huttenhower, D. Gevers, T. W. Cullen, M. Knip and R. J. Xavier, *Cell*, 2016, **165**, 842–853.
33 S. Elizabeth, PhD thesis, University of North Carolina at Chapel Hill, 2013, pp. 1965–1985.
34 A. Weintraub, U. Zähringer, H. -W Wollenweber, U. Seydel and E. T. Rietschel, *Eur. J. Biochem.*, 1989, **183**, 425–431.
35 F. Di Lorenzo, A. Silipo, T. Matier, A. Hanuszkiewicz, J. S. Elborn, R. Lanzetta, L. Sturiale, A. Scamporrino, D. Garozzo, M. A. Valvano, M. M. Tunney and A. Molinaro, *Eur. J. Org Chem.*, 2016, 1732–1738.
36 K. Hiippala, V. Kainulainen, M. Suutarinen, T. Heini, J. R. Bowers, D. Jasso-Selles, D. Lemmer, M. Valentine, R. Barnes, D. M. Engelthaler and R. Satokari, *Nutrients*, 2020, **12**, 935.
37 J. Pazol, T. M. Weiss, C. D. Martínez, O. Quesada and E. Nicolau, *JCIS Open*, 2022, **7**, 100058.
38 M. Vaccaro, A. Accardo, D. Tesauro, G. Mangiapia, D. Löf, K. Schillén, O. Söderman, G. Morelli and L. Paduano, *Langmuir*, 2006, **22**, 6635–6643.
39 A. E. Mohr, M. Crawford, P. Jasbi, S. Fessler and K. L. Sweazea, *FEBS Lett.*, 2022, **596**, 849–875.
40 L. Hong, M. Gontsarik, H. Amenitsch and S. Salentinig, *Small*, 2022, **18**, 2104211.
41 M. A. Campanero-Rhodes, I. Kalograiaki, B. Euba, E. Llobet, A. Ardá, J. Jiménez-Barbero, J. Garmendia and D. Solís, *Biomolecules*, 2021, **11**, 595.
42 F. Nieto-Fabregat, M. Mercogliano, A. Cangiano, G. Vitiello, E. Andretta, L. A. Clifton, A. Vanacore, L. Buono, M. A. Campanero-Rhodes, D. Solís, C. Di Carluccio, G. Pecoraro, A. Molinaro, G. Smaldone, J. K. Kim, D. H. Kim, L. Paduano, F. Di Lorenzo and A. Silipo, *JACS Au*, 2025, **5**, 3311–3327.
43 M. L. Henriksen, J. Brandt, S. S. C. Iyer, N. M. Thielens and S. Hansen, *Mol. Immunol.*, 2013, **56**, 757–767.
44 Y. Zheng, J. Su, M. C. Miller, J. Geng, X. Xu, T. Zhang, M. Mayzel, Y. Zhou, K. H. Mayo and G. Tai, *Glycobiology*, 2021, **31**, 341–350.
45 M. E. Abouelela and Y. A. Helmy, *Microorganisms*, 2024, **12**, 430.
46 N. J. Foegeding and M. X. Byndloss, *Cell Host Microbe*, 2021, **29**, 851–853.

47 C. Xing, M. Wang, A. A. Ajibade, P. Tan, C. Fu, L. Chen, M. Zhu, Z. Z. Hao, J. Chu, X. Yu, B. Yin, J. Zhu, W. J. Shen, T. Duan, H. Y. Wang and R. F. Wang, *Cell Host Microbe*, 2021, **29**, 959–974.

48 O. Westphal, O. Lüderitz, F. Bister and B. Naturforsch, *J. Chem. Sci.*, 1965, **7**, 148–155.

49 M. D. Pither, A. Silipo, A. Molinaro and F. Di Lorenzo, *Methods Mol. Biol.*, 2023, **2613**, 153–179.

50 F. D. Lorenzo, L. Sturiale, A. Palmigiano, L. Lembo-Fazio, I. Paciello, C. P. Coutinho, I. Sá-Correia, M. L. Bernardini, R. Lanzetta, D. Garozzo, A. Silipo and A. Molinaro, *ChemBioChem*, 2013, **14**, 1105–1115.

51 F. D. Lorenzo, A. Palmigiano, I. Paciello, M. Pallach, D. Garozzo, M. L. Bernardini, V. Cono, M. M. Yakimov, A. Molinaro and A. Silipo, *Mar. Drugs*, 2017, **15**(7), 201.

52 L. De Simone Carone, G. Barra, R. Cirella, M. Ziaco, M. Mercogliano, F. Olmeo, E. Andretta, V. Mazziotti, C. Fusco, G. D'Ippolito, K. A. Duda, F. M. Farquharson, P. Louis, A. Fontana, A. Silipo, A. Molinaro, F. Chiodo and F. Di Lorenzo, *Angew. Chem., Int. Ed.*, 2025, e202512947.

53 F. Di Lorenzo, *Antonie van Leeuwenhoek*, 2017, **110**, 1401–1412.

54 J. K. Kim, H. A. Jang, M. S. Kim, J. H. Cho, J. Lee, F. Di Lorenzo, L. Sturiale, A. Silipo, A. Molinaro and B. L. Lee, *J. Biol. Chem.*, 2017, **292**, 19226–19237.

55 A. Cangiano, N. Gallucci, A. Giarra, J. Ali, L. Chiappisi, N. P. Cowieson and L. Paduano, *Nanoscale*, 2025, **17**, 15829–15840.

56 N. P. Cowieson, C. J. C. Edwards-Gayle, K. Inoue, N. S. Khunti, J. Doutch, E. Williams, S. Daniels, G. Preece, N. A. Krumpa, J. P. Sutter, A. D. Tully, N. J. Terrill and R. P. Rambo, *J. Synchrotron Radiat.*, 2020, **27**, 1438–1446.

57 N. Gallucci, M. S. Appavou, N. Cowieson, G. D'Errico, R. Di Girolamo, S. Lettieri, F. Sica, G. Vitiello and L. Paduano, *J. Colloid Interface Sci.*, 2024, **659**, 926–935.

58 M. A. Campanero-Rhodes, R. A. Childs, M. Kiso, S. Komba, C. Le Narvor, J. Warren, D. Otto, P. R. Crocker and T. Feizi, *Biochem. Biophys. Res. Commun.*, 2006, **344**, 1141–1146.